

## Synthesis, physicochemical properties and antimicrobial activity of mono-/dinitroxyl amides†‡

Miroslav Kavala,<sup>a</sup> Vlasta Brezová,<sup>b</sup> Ľubomír Švorc,<sup>c</sup> Zuzana Vihonská,<sup>d</sup> Petra Olejníková,<sup>d</sup> Ján Moncol,<sup>e</sup> Jozef Kožíšek,<sup>b</sup> Peter Herich<sup>b</sup> and Peter Szolcsányi<sup>\*a</sup>

Two comparative sets of mono-/dinitroxyl amides were designed and prepared. The novel TEMPO and/or PROXYL derivatives were fully characterised and their spin, redox and antimicrobial properties were determined. Cyclic voltammetry revealed (quasi)reversible redox behavior for most of the studied radicals. Moreover, the electron-withdrawing substituents increased the oxidation potential of nitroxides in comparison to electron-donating groups. While EPR spectra of monoradicals featured the typical three-line signal, the spectra of biradicals showed more complex splitting patterns. The *in vitro* biological assay revealed that unlike pyrrolidinyl derivatives, the piperidinyl nitroxides significantly inhibited the growth of *Staphylococcus* sp.

Received 10th February 2014,  
Accepted 9th April 2014

DOI: 10.1039/c4ob00302k

www.rsc.org/obc

## Introduction

The amidic derivative of 4-amino-TEMPO (*N*-acetylamino-2,2,6,6-tetramethylpiperidine-*N*-oxide, AA-TEMPO, Fig. 1) has recently been identified as a promising oxidation catalyst.<sup>1</sup> This stable nitroxide is currently produced on an industrial scale as an emerging substitute for the widely used radical oxidant TEMPO<sup>2,3</sup> (Fig. 1).

Despite the lack of  $\pi$ -conjugation in their saturated skeletons, various TEMPO derivatives show a clear dependence of

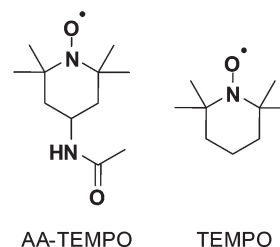


Fig. 1 Nitroxide-type oxidation catalysts.

their physicochemical properties (stemming from the presence of a radical site) on the electronic nature of C-4 substituents.<sup>4,5</sup> An in-depth insight into these effects is crucial for the rational design and practical utilisation of stable nitroxides<sup>6</sup> as prospective functional materials including radical batteries,<sup>7</sup> magneto-active compounds,<sup>8</sup> redox mediators in dye-sensitised solar cells,<sup>9</sup> and/or multi-responsive copolymers.<sup>10</sup> Moreover, there is an emerging range of medicinal applications of low-toxic nitroxides as fMRI contrast enhancing<sup>11</sup> and radiation protective agents,<sup>12</sup> topical drugs for alopecia prevention,<sup>13</sup> and/or antioxidants displaying antihypertensive effects.<sup>14</sup> Within this broad context, we are interested in the targeted design, practical synthesis and property evaluation of novel mono/dinitroxyl amides inspired by AA-TEMPO. Thus, we have designed and prepared a series of novel mononitroxyl amides/carbamates 4–9 and dinitroxyl amides/ureas 10–13 as two comparative sets and systematically investigated the influence of (stereo)electronic effects of *N*-substituents and/or nitroxide

<sup>a</sup>Department of Organic Chemistry, Slovak University of Technology in Bratislava, Radlinského 9, SK-812 37 Bratislava, Slovakia. E-mail: peter.szolcsanyi@stuba.sk

<sup>b</sup>Department of Physical Chemistry, Slovak University of Technology in Bratislava, Radlinského 9, SK-812 37 Bratislava, Slovakia

<sup>c</sup>Department of Analytical Chemistry, Slovak University of Technology in Bratislava, Radlinského 9, SK-812 37 Bratislava, Slovakia

<sup>d</sup>Department of Biochemistry and Microbiology, Slovak University of Technology in Bratislava, Radlinského 9, SK-812 37 Bratislava, Slovakia

<sup>e</sup>Department of Inorganic Chemistry, Faculty of Chemical and Food Technology, Slovak University of Technology in Bratislava, Radlinského 9, SK-812 37 Bratislava, Slovakia

† Dedicated to the memory of Peter Tisovský.

‡ Electronic supplementary information (ESI) available: Copies of CV spectra of all nitroxides 4–13; copies of EPR spectra of mononitroxides 4–9; EPR spectra of dinitroxide 11 in DCM fresh solution and after 1-month storage at +4 °C, EPR spectra of dinitroxide 11 in DMSO in the temperature range of 298 K–373 K, copies of HRMS spectra of nitroxides 8, 9 and 11; ORTEP drawings and/or packing diagrams of nitroxides 4, 5, 8, 10, 11 and their selected crystallographic data. CCDC 953446 (for 4), 953447 (for 5), 953448 (for 8), 953449 (for 10), and 953450 (for 11·0.5EtOH·0.5H<sub>2</sub>O). For ESI and crystallographic data in CIF or other electronic format see DOI: 10.1039/c4ob00302k

ring size on the spectroscopic properties, electrochemical behaviour as well as potentially useful biological activity of the studied compounds.

## Results and discussion

### Synthesis

While the starting mononitroxides 4-amino-TEMPO **1** and 3-amino-PROXYL **2** are commercially available, the known dinitroxide **3** was readily prepared *via* a modified<sup>5</sup> synthetic protocol.<sup>15</sup> All three starting radicals **1–3** (Fig. 2) are sufficiently stable under standard storage conditions and do not readily decompose even at slightly elevated temperature.<sup>16</sup>

Thus, employing **1** and **2** as substrates, we have designed and prepared a set of *N*-substituted TEMPO **4–8** and PROXYL **9** monoradicals. For comparison purposes, we have chosen bulky pivaloyl amide **4**<sup>17</sup> and carbamate **5**,<sup>18</sup> electron-donating benzamide **6** and formamide **7**,<sup>19</sup> and electron-withdrawing trifluoroacetamides **8**<sup>20</sup> and **9**. The synthesis of all mononitroxides consisted of a standard one-step *N*-carbonylation with either chlorides, anhydrides and/or formate as corresponding electrophiles. The desired amidic derivatives **4–9** were obtained at high purity in good to excellent yields (72–93%) after FLC (Scheme 1).

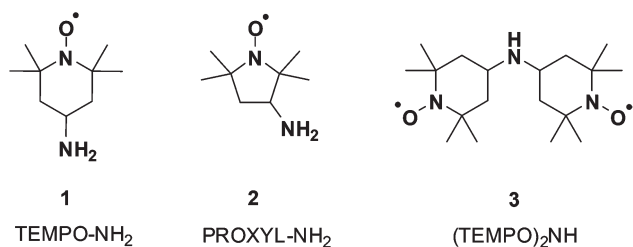
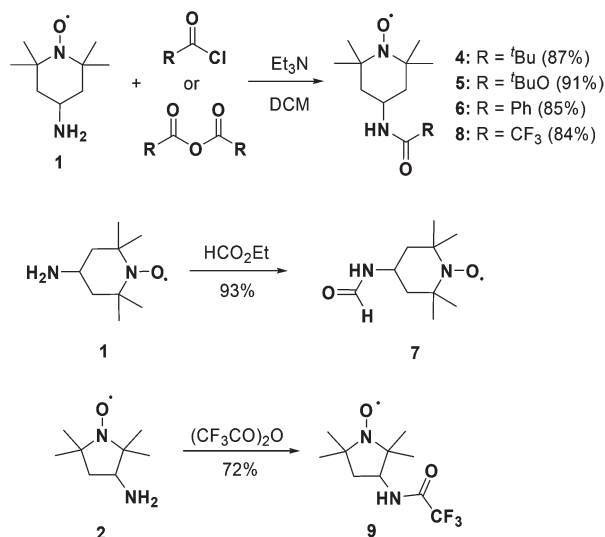


Fig. 2 Starting aminonitroxides **1–3**.

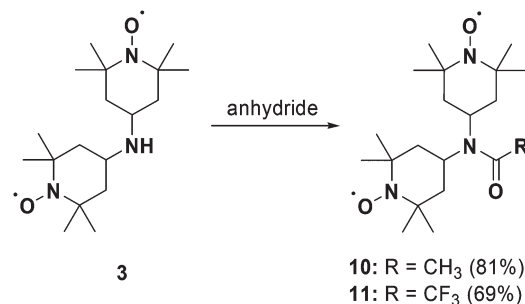


Scheme 1 Synthesis of mononitroxides **4–9**.

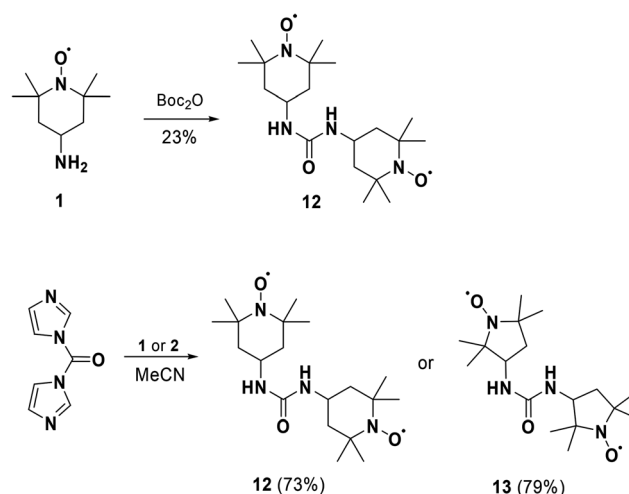
In order to compare the properties of amidic mono- vs. biradicals, we have used tertiary amides **10** and **11**. Analogously to the abovementioned mononitroxides, biradicals **10** and **11** were prepared from bis-TEMPO-amine **3** by its carbonylation with the corresponding anhydrides in the presence of triethylamine in good to moderate yield (81% resp. 69%, Scheme 2).

Finally, to examine the influence of a 6- vs. a 5-membered ring on the physicochemical properties of dinitroxides, we prepared bis-TEMPO and bis-PROXYL ureas **12** and **13**. While the original carbonylative conditions<sup>21</sup> (Boc<sub>2</sub>O, DMAP, MeCN) provided the desired derivative **12** in 23% yield only, our modified synthetic protocol involving 1,1'-carbonyldiimidazole (CDI) as a coupling reagent furnished both ureas **12** and **13** in good yields (Scheme 3).

Having prepared the desired amidic mono-/biradicals **4–13**, we investigated their spectroscopic (EPR) and electrochemical (CV) properties. In addition, we have screened all compounds *in vitro* for their potentially useful antimicrobial activities. We have also performed single-crystal X-ray analyses of mono-/dinitroxides **4**, **5**, **8**, **10**, **11** and elucidated their solid state structures.



Scheme 2 Synthesis of dinitroxides **10** and **11**.



Scheme 3 Optimised synthesis of dinitroxides **12** and **13**.

### Cyclic voltammetry

The redox potentials of the mono-/biradicals **4–13** were determined by cyclic voltammetry (CV) in phosphate buffer solution (PBS, pH 7.0), using a paraffin impregnated graphite electrode (PIGE).<sup>5</sup> In general, nitroxides are readily electrochemically oxidised to the corresponding *N*-oxoammonium cations.<sup>22</sup> Cyclic voltammograms of **4–13** (Fig. S1 in ESI†) reveal that all of the studied compounds undergo an one-electron transfer process with half-wave potentials ( $E_{1/2}$ ) in the range of 582–669 mV vs. Ag/AgCl electrode (Table 1).

Interestingly, while the majority of prepared monoradicals (**5**, **7–9**) showed (quasi)reversible redox properties (**4** and **6** being exceptions) as reflected by the approximately equal anodic and cathodic peak current values ( $I_{pa}/I_{pc} \sim 1.3$ – $1.6$ , Table 1), all biradicals (**11–13**) except one (**10**) exhibited current intensities sufficiently far from equal ( $I_{pa}/I_{pc} \sim 1.9$ – $2.0$ , Table 1), and thus, indicating a significant loss of the kinetic reversibility.<sup>29</sup> However, the cyclic voltammograms of mononitroxides **4–9** and dinitroxides **10–13** are analogous throughout the series (Fig. S1 in ESI†), thus demonstrating that electrochemical oxidation of biradicals **10–13** likely involves simultaneous one-electron transfer to both radical centers rather than a stepwise process. Moreover, CV results again confirmed a recently postulated<sup>9d</sup> and experimentally observed<sup>5</sup> trend that the presence of electron-withdrawing substituents tends to increase the oxidation potential of a nitroxide in comparison to electron-donating groups (cf. **1** vs. **8**, **2** vs. **9**, **10** vs. **11**, Table 1). In addition, we have observed exceptionally high values of anodic, cathodic and half-wave potentials for the biradical **11** ( $E_{pa} = 731$ ,  $E_{pc} = 607$ ,  $E_{1/2} = 669$  mV). However, this particular dinitroxide also features not only a large separation of its redox potentials ( $\Delta E = 124$  mV) in comparison to the

theoretical Nernstian value (59 mV), but also a non-equal ratio of anodic and cathodic peak currents ( $I_{pa}/I_{pc} = 2$ ).

### EPR spectroscopy

EPR spectra of mononitroxides **4–9** measured in dichloromethane (DCM) at 295 K under argon are characteristic of typical three-line signals reflecting the interaction of the unpaired electron with a  $^{14}\text{N}$  nucleus ( $A_N$ ) with poorly resolved hyperfine structure caused by  $^1\text{H}$  or  $^{13}\text{C}$  nuclei ( $A_X$ ). The experimental EPR spectra along with their simulations are depicted in Fig. S2 (see ESI†). The spin Hamiltonian parameters elucidated from the simulation of the experimental EPR spectra are summarised in Table 2.

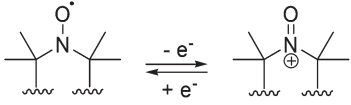
In contrast to mononitroxides **4–9**, the EPR spectra of dinitroxides **10–13** obtained in DCM under argon at 295 K revealed different splitting patterns (Fig. 3 and 4), thus reflecting the variations in their structures. The spin Hamiltonian for a nitroxide biradical can be constructed with the terms representing the electron Zeeman interactions with an external magnetic field, the hyperfine interactions of each electron with the nuclear spins, and the exchange coupling of the two electron spins (eqn (1)):<sup>30a</sup>

$$H = g^{(1)}\beta_e B S_z^{(1)} + g^{(2)}\beta_e B S_z^{(2)} + A^{(1)}I_z^{(1)}S_z^{(1)} + A^{(2)}I_z^{(2)}S_z^{(2)} + JS_z^{(1)}S_z^{(2)} \quad (1)$$

where  $g^{(1)}\beta_e B S_z^{(1)} + g^{(2)}\beta_e B S_z^{(2)}$  is the Zeeman coupling between the unpaired electrons spin and the magnetic field  $B$ ;  $A^{(1)}I_z^{(1)}S_z^{(1)} + A^{(2)}I_z^{(2)}S_z^{(2)}$  is the hyperfine interaction of the electron spins with magnetically active nuclei, one  $^{14}\text{N}$  nucleus is characterised with a hyperfine coupling constant  $A_N^{(1)}$  or  $A_N^{(2)}$  considering the vicinity of one unpaired electron for dinitroxide; and the last component  $JS_z^{(1)}S_z^{(2)}$  represents the exchange coupling between two electron spins, where  $J$  is the exchange coupling constant.<sup>30b</sup>

For the dinitroxides possessing two symmetric nitroxide moieties in the isotropic solutions the  $g$ -values in the spin Hamiltonian may be identical ( $g^{(1)} = g^{(2)}$ ), along with the same values of nitrogen hyperfine coupling constants ( $A_N^{(1)} = A_N^{(2)}$ ). However, the specific interactions of the  $\text{NO}^\bullet$  group with solvent molecules may cause small asymmetry ( $g^{(1)} \neq g^{(2)}$ ).

**Table 1** Experimental redox potentials and current responses of nitroxide/*N*-oxoammonium cation redox couples

Nitroxide			$E_{1/2}^c$ (mV)	$\Delta E^d$ (mV)	$I_{pa}/I_{pc}^e$
	$E_{pa}^a$ (mV)	$E_{pc}^b$ (mV)			
<b>1</b> <sup>23–26</sup>	652	582	617	69	1.0
AA-TEMPO <sup>24,27</sup>	620	550	585	70	1.0
<b>2</b> <sup>28</sup>	684	556	620	128	1.1
<b>3</b> <sup>5</sup>	574	466	520	108	1.2
<b>4</b>	638	538	588	100	1.9
<b>5</b>	680	526	603	154	1.3
<b>6</b>	695	515	605	180	2.1
<b>7</b>	650	538	594	112	1.5
<b>8</b>	668	538	603	130	1.5
<b>9</b>	692	584	638	108	1.6
<b>10</b>	685	545	615	140	1.5
<b>11</b>	731	607	669	124	2.0
<b>12</b>	633	531	582	102	2.0
<b>13</b>	628	554	591	75	1.9

<sup>a</sup>  $E_{pa}$  = anodic peak potential. <sup>b</sup>  $E_{pc}$  = cathodic peak potential. <sup>c</sup>  $E_{1/2}$  =  $(E_{pa} + E_{pc})/2$ . <sup>d</sup>  $\Delta E = E_{pa} - E_{pc}$ . <sup>e</sup>  $I_{pa}$  = anodic peak current,  $I_{pc}$  = cathodic peak current.

**Table 2** Hyperfine coupling constants (mT, accuracy  $\pm 0.001$ ) and  $g$ -values (accuracy  $\pm 0.0001$ ) elucidated from the simulation of the experimental EPR spectra of monoradicals **4–9** measured in DCM at 295 K under Ar

Nitroxide	$A_N$ (mT)	$A_X$ (mT)	$g$ -value
<b>4</b>	1.581	—	2.0061
<b>5</b>	1.583	0.047 (6H), 0.037 (6H) 0.016 (2H), 0.004 (2H)	2.0061
<b>6</b>	1.581	0.043 (6H), 0.040 (6H) 0.017 (2H), 0.011 (2H)	2.0061
<b>7</b>	1.581	0.042 (6H), 0.040 (6H) 0.017 (2H), 0.010 (2H)	2.0061
<b>8</b>	1.573	0.045 (6H), 0.038 (6H) 0.016 (2H), 0.005 (2H)	2.0061
<b>9</b>	1.444	0.892 ( $^{13}\text{C}$ ), 0.500 ( $^{13}\text{C}$ )	2.0058

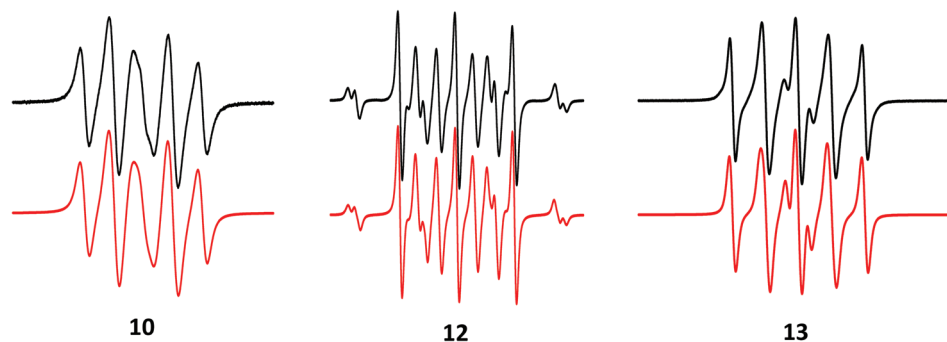


Fig. 3 Experimental (–) and simulated (–) X-band EPR spectra of dinitroxides **10**, **12** and **13** obtained at 295 K in DCM. Magnetic field sweep 7 mT; dinitroxide concentration 0.1 mM.

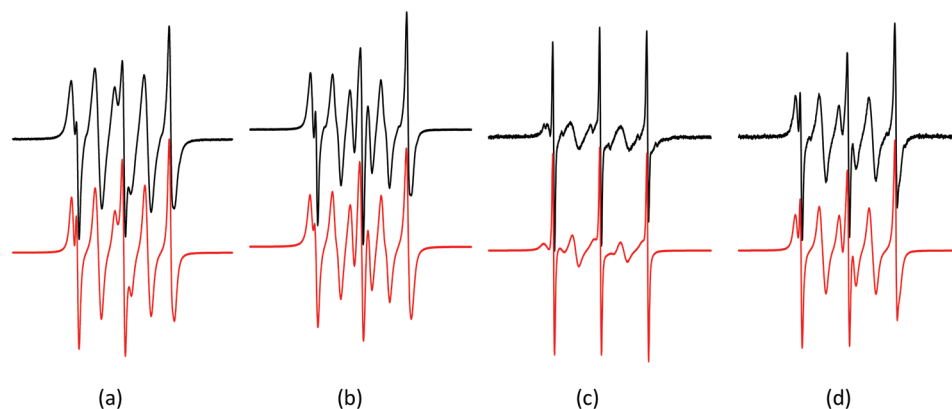


Fig. 4 Experimental (–) and simulated (–) X-band EPR spectra of dinitroxide **11** (magnetic field sweep 7 mT; dinitroxide concentration 0.1 mM) obtained under Ar at 295 K in: (a) DCM at 295 K, (b) *n*-heptane at 295 K, (c) DMSO at 295 K, and (d) DMSO at 373 K.

and  $A_N^{(1)} \neq A_N^{(2)}$  which is also the case for symmetric dinitroxide molecules.<sup>5,30</sup>

In general, the EPR spectra of nitroxide biradicals are substantially influenced by the value of the exchange coupling constant.<sup>30</sup> Two limiting situations may be considered here:  $J = 0$  where each nitroxide moiety separately contributes to the EPR signal giving a three-line spectrum (intensity ratio 1 : 1 : 1), and  $J \gg A_N$  representing the interacting electrons with a five-line EPR spectrum (intensity ratio 1 : 2 : 3 : 2 : 1). However, if  $J \sim A_N$  the EPR spectra of dinitroxides are complex as shown in Fig. 3 for dinitroxide **12**.

The data elucidated from the simulation of the experimental EPR spectra of dinitroxides **10–13** measured in DCM under argon at 295 K are summarised in Table 3.

Thus, the five-line EPR spectrum of biradical **10** corresponds well to the value of  $J/A_N > 10$  (Fig. 3, Table 3); the asymmetry found for the  $A_N$  couplings is most probably caused by the interaction of nitroxide moieties with polar solvent molecules (DCM); an associated phenomenon was generally observed earlier by others<sup>30</sup> and confirmed recently by our DFT and/or MP2 calculations.<sup>5</sup> On the other hand, in order to fit with the experiment, the simulated EPR spectrum of **11** (Fig. 4) was constructed as a superposition of two different signals corresponding to interacting and non-interacting radicals<sup>31</sup> within the molecule of the respective dinitroxide. In

Table 3 Hyperfine coupling constants (mT, accuracy  $\pm 0.001$ ), exchange coupling constant (MHz, accuracy  $\pm 10\%$ ) and *g*-values (accuracy  $\pm 0.0001$ ) elucidated from the simulation of the experimental EPR spectra of biradicals **10–13** measured in DCM at 295 K under argon, along with the averaged *g*-values ( $g_{av}$ )

Nitroxide	$A_N$ (mT)	$J^b$ (MHz)	<i>g</i> -value	$g_{av}$
<b>10</b>	1.521, 1.642	$\sim 360$	2.0064, 2.0067	2.0066
<b>11</b>	1.639, 1.539 <sup>a</sup>	$\sim 410$	2.0064, 2.0065	2.0065
	1.486 <sup>a</sup>	0	2.0063	2.0063
<b>11<sup>c</sup></b>	1.552, 1.530 <sup>a</sup>	$\sim 240$	2.0067, 2.0065	2.0066
	1.443 <sup>a</sup>	0	2.0064	2.0064
<b>11<sup>d</sup></b>	1.582, 1.590 <sup>a</sup>	$\sim 350$	2.0065, 2.0062	2.0064
	1.506 <sup>a</sup>	0	2.0062	2.0062
<b>12</b>	1.586, 1.585	$\sim 50$	2.0068, 2.0061	2.0065
<b>13</b>	1.370, 1.549	$\sim 430$	2.0060, 2.0063	2.0062

<sup>a</sup> Superposition of the signals of interacting and non-interacting biradicals of amide **11**. <sup>b</sup> 1 mT = 28.0 MHz ( $g = 2$ ). <sup>c</sup> Measured in *n*-heptane at 295 K. <sup>d</sup> Measured in dimethylsulfoxide at 373 K.

order to obtain more information about the potential influence of the conformational dynamics of dinitroxide **11** in solution, we measured its EPR spectra at 295 K in non-polar *n*-heptane, as well as in the more viscous and polar dimethylsulfoxide within the temperature range of 298 K–373 K (Fig. 4). The EPR spectrum of **11** measured in *n*-heptane is compatible



with the spectrum measured in DCM under identical experimental conditions, and thus, represents the superposition of two individual signals. Due to the reduced solvent polarity, the nitrogen hyperfine couplings in *n*-heptane are lower, and the differences between individual  $A_N^{(i)}$  and  $g^{(i)}$  are not noticeable (Table 3). A three-line signal of the non-interacting component ( $J = 0$ ) dominates the EPR spectrum of **11** measured at room temperature in viscous DMSO, while a conformer ratio comparable with the one observed in DCM or *n*-heptane was obtained only at 373 K in DMSO (Fig. S3 in ESI†). Interestingly, the original conformer ratio of 1 : 1 found in the freshly prepared DCM solution of **11** was changed to a ratio of 1 : 3 in the DCM solution stored for one month at +4 °C (Fig. S4 in ESI†).

Moreover, the influence of 6- vs. 5-membered rings on the EPR spectra of biradicals **12** and **13** was analysed. While *N,N'*-bis-TEMPO urea **12** is characterised by a limited exchange coupling between two nitroxide moieties ( $J/A_N \sim 1$ ), and thus, shows a rather complex<sup>32</sup> EPR spectrum (Fig. 3), the five-line EPR spectrum of *N,N'*-bis-PROXYL urea **13** was successfully simulated with  $J/A_N > 10$  (Table 3). Here, the diminished exchange coupling obtained for biradical **12** probably reflects the increased distance<sup>33</sup> between its two nitroxide groups in comparison to biradical **13**.

### X-ray diffraction studies

In order to obtain a detailed insight into the molecular and bulk structures of the studied mono-/biradicals in the solid phase, the X-ray analyses of single crystals of mononitroxides **4**, **5**, and **8** as well as dinitroxides **10** and **11** were performed (the crystallographic data are summarised in Table S1 in ESI†). The ORTEP drawings of elucidated crystal structures are depicted in Fig. 5–9. As expected, the piperidine rings in all of these compounds exhibit a chair conformation. Moreover, all nitroxides are stabilised by networks of intra-/intermolecular hydrogen bonds and/or weak interactions in their crystal packings (Fig. S5–S14 in ESI†). The selected parameters of hydrogen bonds and interactions are summarised in Table S2 (see ESI†). In all studied cases, the nitroxyl N–O<sup>•</sup> bond lengths follow a standard interatomic distance ( $\sim 1.28$  Å, Table 4) observed for similar TEMPO derivatives.<sup>5</sup> While the amidic C=O bond lengths in nitroxides **4**, **8**, **10** and **11** fall into the

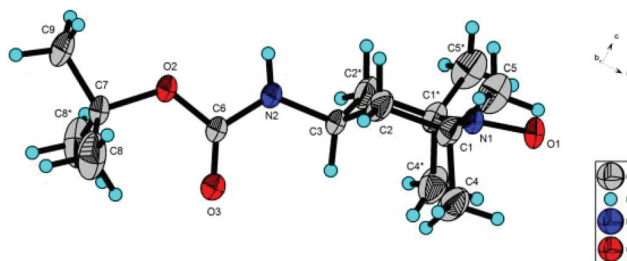


Fig. 6 ORTEP drawing of mononitroxide **5**.

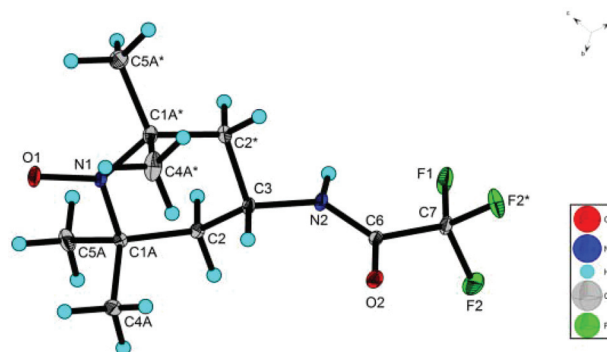


Fig. 7 ORTEP drawing of mononitroxide **8**.

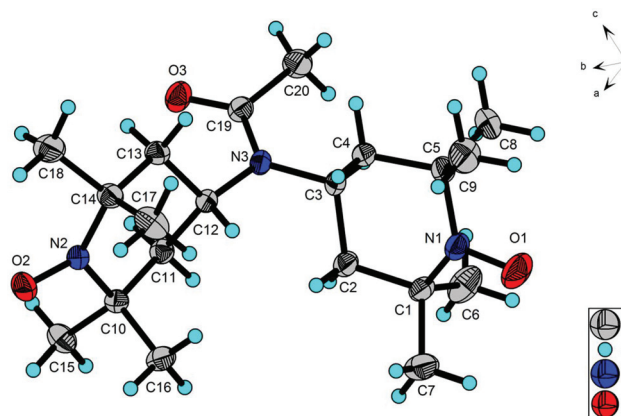


Fig. 8 ORTEP drawing of dinitroxide **10**.

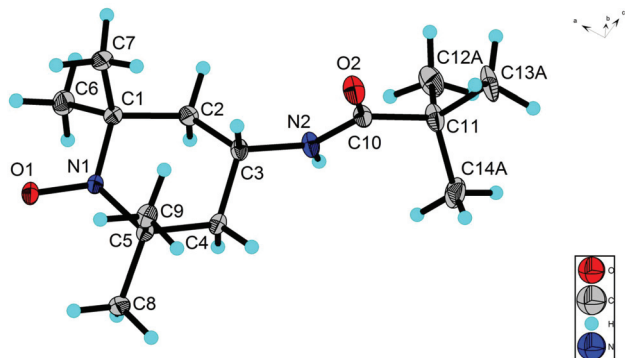


Fig. 5 ORTEP drawing of mononitroxide **4**.

range of 1.20–1.25 Å usually observed for carbonylamino groups,<sup>34</sup> an analogous interatomic distance in carbamate **5** (1.191(3) Å) is expectedly shorter (Table 4). Accordingly, the C–N bond distances of carbonylamino groups in all studied nitroxides are in the standard range of 1.32–1.38 Å usually observed<sup>34</sup> for carboxamides (Table 4).

Due to the significant rotational flexibility of the *tert*-butyl group in amide **4** (Fig. 5) the X-ray analysis furnished an ORTEP with disordered parts (Fig. S5 in ESI†). From the bulk point of view, single molecules of mononitroxide **4** are interconnected *via* hydrogen bonds between the carboxamide group into the supramolecular *C*(4) chains<sup>35</sup> with a H $\cdots$ O distance of 2.120 Å (Fig. S6 in ESI†).

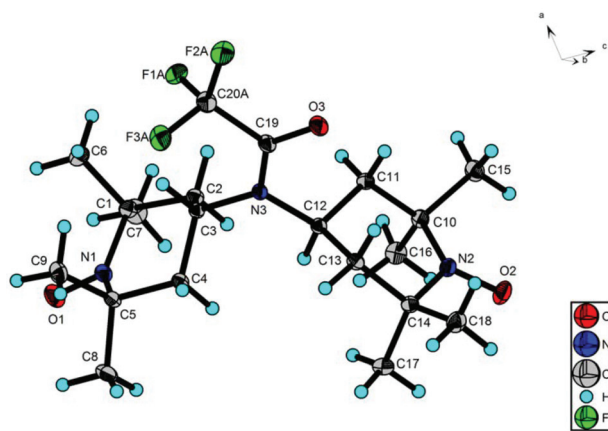


Fig. 9 ORTEP drawing of dinitroxide **11·0.5EtOH·0.5H<sub>2</sub>O**. The solvent molecules (EtOH and H<sub>2</sub>O) were omitted for clarity.

Table 4 Comparison of bond lengths obtained from X-ray analyses

Nitroxide	N–O <sup>•</sup> (Å)	C=O (Å)	C–N (Å)
<b>4</b>	1.283(2)	1.220(2)	1.318(2)
<b>5</b>	1.285(2)	1.191(3)	1.327(3)
<b>8</b>	1.288(3)	1.203(4)	1.324(4)
<b>10</b>	1.282(2)	1.222(2)	1.360(2)
<b>11<sup>a</sup></b>	1.282(2)	1.218(3)	1.342(3)

<sup>a</sup> The crystal of dinitroxide **11** included ethanol and water as solvent molecules (**11·0.5EtOH·0.5H<sub>2</sub>O**).

The symmetrical molecule of mononitroxide **5** (Fig. 6) lies in mirror spaces and two halves of the molecule occupy independent parts of the cell. The bulk structure of **5** is stabilised by both intermolecular NH...O hydrogen bonds between the nitroxyl and carbamate moieties (2.055 Å), and three types of H...H intermolecular contacts (H2B and H4B, H8B and H5A, H5B and H9A) with interatomic distances in the range of 2.474–2.870 Å (Fig. S7 in ESI†).

Analogously to **5**, the symmetrical molecule of mononitroxide **8** (Fig. 7) also lies in mirror spaces and two halves of the molecule occupy independent parts of the cell. Moreover, due to the rotational flexibility of the CF<sub>3</sub>-group, the X-ray analysis of trifluoroacetamide **8** furnished an ORTEP with disordered parts (Fig. S8 in ESI†). The bulk structure of **8** consists of zig-zag 1-D supramolecular C(7) chains<sup>35</sup> formed by intermolecular NH...O hydrogen bonds between the nitroxyl and amide moieties with a distance of 2.000 Å (Fig. S9 in ESI†). The molecular network of **8** also features weak C–H...O hydrogen bonds with interatomic distances of 2.636 and 2.717 Å, respectively.

The bulk structure of dinitroxide **10** (Fig. 8) is stabilised by intramolecular H...H interactions with a very short interatomic distance of 1.978 Å (between H12A and H2B) and seven intermolecular interactions: between the nitroxyl's oxygen and hydrogen atoms H6B, H20B, H16B, H17A (2.469–2.822 Å), between amidic oxygen O3 and H4A (2.672 Å), H15A and H18B, H13B with interatomic distances of 2.420 and 2.325 Å (Fig. S10–S12 in ESI†).

The X-ray analysis of a crystal obtained by slow evaporation of a wet ethanolic solution of dinitroxide **11** (Fig. 9) revealed that both EtOH and H<sub>2</sub>O were incorporated into the solid during its formation to yield **11·0.5EtOH·0.5H<sub>2</sub>O**. Due to the rotational flexibility of the CF<sub>3</sub>-group, the X-ray analysis of trifluoroacetamide **11** furnished an ORTEP with disordered parts (Fig. S13 in ESI†). On the other hand, the disordered solvent molecules around special positions are connected to the dinitroxide **11** through O1W–H1WA...O1S, O1W–H1WB...O2 and O1S–H1S...O1W hydrogen bonds with H...O distances in the range of 2.190–2.390 Å. The O–H...O network is completed by a weak C7–H7A...O1S hydrogen bond with a H7A...O1S distance of 2.571 Å (Fig. S14 in ESI†). Regarding the bulk structure, the molecules of **11** are linked through weak C2–H2B...O3 and C11–H11B...F2A interactions into supramolecular zig-zag chains with H...O/F distances of 2.564 and 2.615 Å, respectively.

### Antimicrobial assays *in vitro*

The prepared mononitroxides **4–9** and dinitroxides **10–13** were also tested for their *in vitro* antimicrobial activity (Table 5) using bacteria (*Staphylococcus aureus*, *Staphylococcus epidermidis*, *Proteus* sp.), yeast (*Candida albicans*, *Candida parapsilosis*) and filamentous fungi (*Fusarium culmorum*, *Botrytis cinerea*, *Aspergillus fumigatus*). Considering the antibacterial properties, while all the nitroxide radicals displayed a growth inhibition of prokaryotic Gram-positive *S. epidermidis* (58–88%) and/or *S. aureus* (10–79%), the gamma-proteobacteria *Proteus* sp. was fully resistant to all but one of the tested compounds (22% growth inhibition with dinitroxide **10**) even at 1 mM concentration. Interestingly, the mononitroxide **8** was highly selective against *S. epidermidis* (IC<sub>50</sub> 0.5 mmol L<sup>−1</sup>). In general, this bacterial strain was sensitive towards all piperidinyl nitroxides with the highest antimicrobial effect observed for **5**, **6**, **10**, and **11**. In contrast, neither of the two pyrrolidinyl derivatives **9** and/or **13** were capable of inhibiting the growth of *S. epidermidis*. This observation clearly points to the importance of the

Table 5 The inhibitory effect of mono-/dinitroxides **4–13** on the growth of *Staphylococcus* sp.

Nitroxide	<i>S. aureus</i>		<i>S. epidermidis</i>	
	Inhibition <sup>a</sup> (%)	IC <sub>50</sub> <sup>b</sup> (mmol L <sup>−1</sup> )	Inhibition <sup>a</sup> (%)	IC <sub>50</sub> <sup>b</sup> (mmol L <sup>−1</sup> )
<b>4</b>	10	>1	69	0.4
<b>5</b>	31	>1	88	<0.05
<b>6</b>	24	>1	75	0.09
<b>7</b>	13	>1	58	0.6
<b>8</b>	0	>1	66	0.5
<b>9</b>	12	>1	0	>1
<b>10</b>	74	0.3	75	0.07
<b>11</b>	79	0.05	84	<0.05
<b>12</b>	19	>1	65	0.6
<b>13</b>	21	>1	0	>1

<sup>a</sup> Growth inhibition determined at 1 mmol L<sup>−1</sup> concentration of the tested compound. <sup>b</sup> In all cases, the corresponding MIC values were higher than 1 mmol L<sup>−1</sup>.

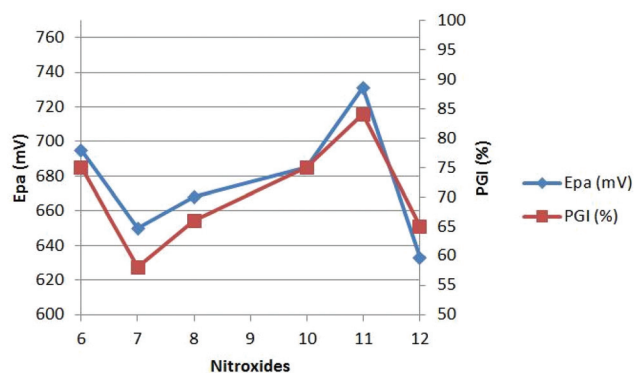


Fig. 10 Correlation of the anodic potential ( $E_{pa}$ ) of piperidine nitroxides 6–8, 10–12 with their growth inhibition (PGI) of *S. epidermidis*.

TEMPO over the PROXYL skeleton in order to suppress this particular bacterial strain. In addition, piperidinyl dinitroxides 10 and 11 were also active against *S. aureus* (Table 5).

Moreover, we have found an interesting correlation<sup>36</sup> between the electronic characteristics of substituents at position C-4 of the piperidine ring (reflected by redox potentials) of TEMPO derivatives 6–8, 10–12 and their *in vitro* inhibition activity against *S. epidermidis* (Fig. 10). It is clear that the more electron-withdrawing substituents (*cf.* 7 *vs.* 8, 10 *vs.* 11) and/or more TEMPO units (*cf.* 8 *vs.* 11) present in the respective nitroxide the stronger is the bacterial growth inhibition. As the anodic potential reflects the ability of a nitroxide to transfer its unpaired electron(s), it appears that the stronger the reductant (higher  $E_{pa}$ ) the better is the growth inhibition (higher PGI). We speculate that such a relationship might suggest a mechanism of antibacterial action *via* an induction/promotion of complex oxidative burst involving highly reactive ROS species.<sup>37</sup>

Regarding the antifungal properties,<sup>38</sup> mono/dinitroxides 4–13 showed only weak to moderate activity. Even though complete growth inhibition was not observed in the range of tested concentrations, however, derivatives 7 and 11 have partially

Table 6 The inhibitory effect of mono-/dinitroxides 4–13 on the growth of filamentous fungi

Nitroxide	Inhibition <sup>a,b</sup> (%)		
	<i>F. culmorum</i>	<i>B. cinerea</i>	<i>A. fumigatus</i>
4	11	13	7
5	27	17	11
6	21	50	15
7	51	8	7
8	16	4	9
9	22	15	7
10	17	8	9
11	52	27	26
12	7	39	9
13	19	39	9

<sup>a</sup>Growth inhibition determined at 1 mmol L<sup>-1</sup> concentration of the tested compound. <sup>b</sup>In all cases, the corresponding MIC values were higher than 1 mmol L<sup>-1</sup>.

suppressed the growth of *F. culmorum* (~50% inhibition), analogously to compound 6 that was moderately active against *B. cinerea*. On the other hand, however, all tested compounds generally showed only (very) weak inhibition activity towards *A. fumigatus* (Table 6). Finally, model yeasts were primarily resistant to any of the tested mono/dinitroxides (0–17% inhibition at 1 mmol L<sup>-1</sup>) except biradical 13 that was able to partially suppress the growth of *C. parapsilosis* (27% inhibition).

## Conclusions

In conclusion, two comparative sets of mononitroxyl amides/carbamates 4–9 and dinitroxyl amides/ureas 10–13 were designed and prepared. These novel TEMPO and/or PROXYL derivatives were fully characterised and some of their solid structures were determined by single crystal X-ray analyses. The spin and redox properties of all the compounds were studied by means of EPR spectroscopy and cyclic voltammetry. In addition, their antimicrobial properties were also investigated. Regarding CV, all studied radicals undergo one-electron transfer process with half-wave potentials in the range of 582–669 mV. The results confirmed an emerging trend that the presence of electron-withdrawing substituents on the saturated N-heterocyclic skeleton tends to increase the oxidation potential of a nitroxide in comparison to electron-donating groups. While EPR spectra of monoradicals 4–9 in DCM feature the typical three-line signal, spectra of biradicals 10–13 revealed more complex splitting patterns. These are most probably caused by the intermolecular interactions of nitroxide moieties with polar solvent molecules and/or conformational flexibility of two radical centres within respective molecules. Moreover, the increased distance between two radical sites in bis-TEMPO *vs.* bis-PROXYL derivatives also influences the complexity of the EPR spectra of the former ones. Finally, we have determined the *in vitro* antimicrobial activity of the prepared nitroxides. Unlike pyrrolidinyl derivatives, all the piperidinyl radicals significantly inhibit the growth of *Staphylococcus* sp. Interestingly, the more electron-withdrawing the substituent is present on the piperidine ring, the stronger is the antibacterial effect of the respective nitroxide against *S. epidermidis*. On the other hand, all tested radicals displayed only a weak growth inhibition of yeast and/or filamentous fungi.

## Experimental

### General

**Synthesis.** All solvents of p.a. purity were dried over 4 Å molecular sieves. All other reagents were purchased and used without further purification. Thin layer chromatography (TLC) was performed on aluminium plates pre-coated with 0.2 mm silica gel 60 F254. Flash column liquid chromatography (FLC) was performed on Kieselgel 60 (40–63 μm). Infrared (IR) spectra were recorded on an FTIR spectrometer as films on a diamond sampler (ATR). Melting points were determined on



capillary apparatus and are uncorrected. Liquid chromatography mass spectrometry (LC-MS) analyses were performed on an instrument equipped with a multimode MS detector using the MM ESI/APCI ionisation method (column: Zorbax SB C-8 12.5\_ 2.1 mm, particle size 5  $\mu$ m, eluent: water–MeOH with 0.1%  $\text{HCO}_2\text{H}$ , gradient 0–100% of MeOH for 2.5 min, flow 1.5  $\text{mL min}^{-1}$ ). HRMS spectra were recorded on a TOF-Q instrument and evaluated using Compass DataAnalysis 4.0 software. Elemental analysis was carried out at the Department of Inorganic Chemistry, Slovak University of Technology in Bratislava, Slovakia.

*N*-(1-Oxo-2,2,6,6-tetramethylpiperidin-4-yl)-pivalamide (**4**). Prepared accordingly to the described procedure.<sup>17</sup> Product was isolated as a pale orange solid (714 mg, 87%). Crystallisation of a small amount of **4** from chloroform–hexanes yielded orange crystals suitable for X-ray analysis (Fig. 5).

For **4**:  $R_F$  = 0.64 (EtOAc), mp 179–180 °C [ref. 17, 179 °C]; ESI-MS ( $m/z$ ) = 256.20 [ $M + 1$ ]<sup>+</sup>; IR (ATR):  $\nu_{\text{max}}$  3332, 2972, 2939, 2868, 1631, 1538, 1477, 1464, 1362, 1322, 1213, 1088, 887, 670, 582  $\text{cm}^{-1}$ ; Anal. Calcd for  $\text{C}_{14}\text{H}_{27}\text{N}_2\text{O}_2$  (255.21): C 65.84, H 10.66, N 10.97. Found C 65.89, H 10.65, N 10.93.

4-tert-Butoxycarbonylamino-2,2,6,6-tetramethylpiperidin-1-oxide (**5**). Prepared according to the described procedure.<sup>18</sup> Product was isolated as a pale orange solid (317 mg, 91%). Crystallisation of a small amount of **5** from an <sup>1</sup>octane–chloroform solution (1 : 1) yielded orange crystals suitable for X-ray analysis (Fig. 6).

For **5**:  $R_F$  = 0.85 (EtOAc), m.p. 197–200 °C [ref. 18, 199 °C]; ESI-MS ( $m/z$ ) = 272.3 [ $M + 1$ ]<sup>+</sup>; IR (ATR)  $\nu_{\text{max}}$  3300, 2970, 2942, 1701, 1531, 1459, 1363, 1309, 1240, 1167, 1133, 1014, 900, 869, 638, 569  $\text{cm}^{-1}$ ; Anal. Calcd for  $\text{C}_{14}\text{H}_{27}\text{N}_2\text{O}_3$  (271.20): C 61.96, H 10.03, N 10.32. Found C 61.91, H 9.80, N 10.03.

*N*-(1-Oxo-2,2,6,6-tetramethylpiperidin-4-yl)-benzoylamide (**6**). 4-Amino-TEMPO **1** (171 mg, 1 mmol) was dissolved in toluene (10 mL) and  $\text{Et}_3\text{N}$  (202 mg, 278  $\mu\text{L}$ , 2 mmol) was added. The reaction mixture was cooled in a water bath (15 °C) and a solution of benzoyl chloride (prepared from benzoic acid (122 mg, 1 mmol) and oxalyl chloride (140 mg, 99  $\mu\text{L}$ , 1.1 mmol) in toluene (10 mL)) was added dropwise. After 2 h, DCM (15 mL) and 1 N aq. HCl (10 mL) were added and the mixture was left stirring for 5 min. The organic phase was separated, dried over anhydrous  $\text{Na}_2\text{SO}_4$ , filtered and evaporated *in vacuo*. Purification by FLC furnished **6** (235 mg, 85%) as an orange solid.

For **6**:  $R_F$  = 0.46 (EtOAc–hexanes 1/2), mp 130–132 °C; ESI-MS ( $m/z$ ) = 276.2 [ $M + 1$ ]<sup>+</sup>; IR (ATR)  $\nu_{\text{max}}$  3415, 3352, 3269, 2976, 2933, 1629, 1545, 1491, 1460, 1331, 1242, 1178, 1076, 702, 560  $\text{cm}^{-1}$ ; Anal. Calcd for  $\text{C}_{16}\text{H}_{23}\text{N}_2\text{O}_2$  (275.37): C 69.79, H 8.42, N 10.17. Found C 69.43, H 8.26, N 9.95.

4-Formamido-2,2,6,6-tetramethylpiperidin-1-oxide (**7**). Prepared according to the described procedure.<sup>19</sup> Product was isolated as a pale orange solid (380 mg, 93%).

For **7**:  $R_F$  = 0.17 ( $\text{CHCl}_3$ –EtOAc 1/1), mp 105–107 °C; ESI-MS ( $m/z$ ) = 200.15 [ $M + 1$ ]<sup>+</sup>; IR (ATR)  $\nu_{\text{max}}$  3359, 2979, 2935, 2870, 1669, 1508, 1380, 1244, 1209, 1179, 1093, 647, 441  $\text{cm}^{-1}$ ; Anal. Calcd for  $\text{C}_{10}\text{H}_{19}\text{N}_2\text{O}_2$  (199.15): C 60.27, H 9.61, N 14.06. Found C 60.41, H 9.47, N 14.01.

4-(2,2,2-Trifluoroacetyl-amino)-2,2,6,6-tetramethylpiperidin-1-oxide (**8**). Modifying the described procedure,<sup>20</sup> nitroxide **8** was prepared by reaction of 4-amino-TEMPO **1** (171 mg, 1 mmol) and  $\text{Et}_3\text{N}$  (203 mg, 280  $\mu\text{L}$ , 2 mmol) with  $(\text{CF}_3\text{CO})_2\text{O}$  (420 mg, 282  $\mu\text{L}$ , 2 mmol) in anhydrous DCM (4 mL). After the reaction was complete (6 h, TLC control), the mixture was diluted with DCM (15 mL), washed with 1 N HCl (15 mL), saturated aq.  $\text{NaHCO}_3$  soln (15 mL) and dried over anhydrous  $\text{Na}_2\text{SO}_4$ . After filtration, the evaporation of volatiles *in vacuo* and FLC purification afforded an orange solid (178 mg, 84%). Crystallisation of a small amount of **8** from ethanolic solution gave orange crystals suitable for X-ray analysis (Fig. 7).

For **8**:  $R_F$  = 0.79 (EtOAc–hexanes 1/1), mp 154–156 °C [ref. 20, 149–151 °C]; ESI-MS ( $m/z$ ) = 269.14 [ $M + 2$ ]<sup>+</sup>; IR (ATR)  $\nu_{\text{max}}$  3282, 3093, 2979, 1724, 1556, 1466, 1365, 1176, 1155, 864, 727, 677, 519  $\text{cm}^{-1}$ ; HRMS Calcd for  $\text{C}_{11}\text{H}_{18}\text{F}_3\text{N}_2\text{O}_2$  267.1320. Found 267.13183.

3-(2,2,2-Trifluoroacetyl-amino)-2,2,5,5-tetramethylpyrrolidin-1-oxide (**9**). 3-Amino-PROXYL **2** (400 mg, 1 mmol) and  $\text{Et}_3\text{N}$  (644 mg, 894  $\mu\text{L}$  mmol, 2.5 mmol) were dissolved in anhydrous DCM (20 mL) and  $(\text{CF}_3\text{CO})_2\text{O}$  (1069 mg, 708  $\mu\text{L}$ , 2 mmol) was added dropwise. After the reaction was complete (16 h, TLC control), the mixture was washed with 1 N HCl (15 mL), saturated aq.  $\text{NaHCO}_3$  soln (15 mL) and dried over anhydrous  $\text{Na}_2\text{SO}_4$ . After filtration, the evaporation of volatiles *in vacuo* and FLC purification afforded **9** (467 mg, 72%) as a pale yellow solid.

For **9**:  $R_F$  = 0.47 (EtOAc–DCM 1/2), mp 119–121 °C; ESI-MS ( $m/z$ ) = 255.11 [ $M + 2$ ]<sup>+</sup>; IR (ATR)  $\nu_{\text{max}}$  3329, 2979, 1723, 1703, 1563, 1468, 1365, 1212, 1180, 1152, 879, 681, 664, 518  $\text{cm}^{-1}$ ; HRMS Calcd for  $\text{C}_{10}\text{H}_{16}\text{F}_3\text{N}_2\text{O}_2$  253.1164. Found 253.11598.

*N*-Acetyl-*N,N*-bis-(1-oxo-2,2,6,6-tetramethylpiperidin-4-yl)-amine (**10**). Bis-TEMPO-amine **3** (800 mg, 2.46 mmol) was dissolved in DCM (10 mL) and  $\text{Et}_3\text{N}$  (503 mg, 691  $\mu\text{L}$ , 4.92 mmol) was added. Then,  $\text{Ac}_2\text{O}$  (502 mg, 464  $\mu\text{L}$ , 4.92 mmol) was added dropwise and the reaction mixture was stirred for 16 h. The mixture was diluted with DCM (10 mL) and water (2 mL) with 1 N HCl (2 mL) were added. The organic phase was separated, washed with saturated aq.  $\text{NaHCO}_3$  soln (10 mL), dried over anhydrous  $\text{Na}_2\text{SO}_4$ , filtered and evaporated *in vacuo*. Purification with FLC afforded **10** (731 mg, 81%) as an orange solid. Crystallisation of a small amount of **10** from an <sup>1</sup>octane–chloroform (1/1) solution yielded red crystals suitable for X-ray analysis (Fig. 8).

For **10**:  $R_F$  = 0.42 (EtOAc–hexanes 1/2), mp 192–195 °C; ESI-MS ( $m/z$ ) = 368.30 [ $M + 1$ ]<sup>+</sup>; IR (ATR)  $\nu_{\text{max}}$  2994, 2935, 1645, 1638, 1466, 1433, 1377, 1364, 1356, 1289, 1238, 1206, 1180, 906, 633, 561  $\text{cm}^{-1}$ ; Anal. Calcd for  $\text{C}_{20}\text{H}_{37}\text{N}_3\text{O}_3$  (367.28) C 65.36, H 10.15, N 11.43. Found C 65.22, H 10.23, N 11.38.

*N*-(2,2,2-Trifluoroacetyl)-*N,N*-bis-(1-oxo-2,2,6,6-tetramethylpiperidin-4-yl)-amine (**11**). Bis-TEMPO-amine **3** (150 mg, 0.46 mmol) was dissolved in anhydrous DCM (2 mL) and  $\text{Et}_3\text{N}$  (117 mg, 160  $\mu\text{L}$ , 1.15 mmol) was added. Trifluoroacetic anhydride (194 mg, 128  $\mu\text{L}$ , 0.92 mmol) was added dropwise and the reaction mixture was stirred for 16 h. The mixture was diluted with DCM (10 mL) and water (2 mL) with 1 N HCl



(2 mL) were added. The organic phase was separated, washed with saturated aq.  $\text{NaHCO}_3$  soln (10 mL), dried over anhydrous  $\text{Na}_2\text{SO}_4$ , filtered and evaporated *in vacuo*. Purification with FLC afforded **11** (134 mg, 69%) as an orange oil which slowly solidified upon standing at r.t. for a few days. Crystallisation of a small amount of **11** from its wet ethanolic solution yielded orange-red crystals of **11**·0.5 $\text{H}_2\text{O}$ ·0.5 $\text{EtOH}$  suitable for X-ray analysis (Fig. 9).

For **11**:  $R_F = 0.74$  ( $\text{EtOAc}$ – $\text{CHCl}_3$  1/1), mp 95–97 °C; ESI-MS ( $m/z$ ) = 422.30 [ $\text{M} + 1$ ] $^+$ ; IR (ATR)  $\nu_{\text{max}}$  2976, 2941, 1684, 1471, 1454, 1364, 1324, 1216, 1191, 1147, 1045, 760, 735, 654, 459  $\text{cm}^{-1}$ ; HRMS Calcd for  $\text{C}_{20}\text{H}_{34}\text{F}_3\text{N}_3\text{O}_3$  $^{+}$  421.2552. Found 421.2546.

*N,N*-Bis-(1-oxo-2,2,6,6-tetramethylpiperidin-4-yl)-carbamide (**12**). Carbonyldiimidazole (213 mg, 1.31 mmol) was mixed with MeCN (6 mL) and a solution of 4-amino-TEMPO **1** (450 mg, 2.63 mmol) in MeCN (4 mL) was added dropwise at r.t. After 24 h, DCM (10 mL) and 1 N HCl (10 mL) were added and the mixture was stirred for 5 min. The organic phase was separated and the water phase was extracted with DCM (2 × 10 mL). The combined organic extracts were dried over anhydrous  $\text{Na}_2\text{SO}_4$ , filtered and evaporated *in vacuo*. Purification by FLC furnished **12** (354 mg, 73%) as a dark orange solid.

For **12**:  $R_F = 0.31$  ( $\text{EtOAc}$ ), mp 200–202 °C [ref. 39, 203–204 °C]; ESI-MS ( $m/z$ ) = 369.20 [ $\text{M} + 1$ ] $^+$ ; IR (ATR)  $\nu_{\text{max}}$  3383, 3307, 3271, 2972, 2934, 1728, 1666, 1622, 1558, 1540, 1315, 1231, 1176, 1072, 636, 562, 432  $\text{cm}^{-1}$ ; Anal. Calcd for  $\text{C}_{19}\text{H}_{36}\text{N}_4\text{O}_3$  $^{+}$  (368.28) C 61.93, H 9.85, N 15.20. Found C 61.71, H 9.79, N 15.18.

*N,N*-Bis-(1-oxo-2,2,5,5-tetramethylpyrrolidin-3-yl)-carbamide (**13**). Carbonyldiimidazole (103 mg, 0.64 mmol) was mixed with MeCN (4 mL) and a solution of 3-amino-PROXYL **2** (200 mg, 1.27 mmol) in MeCN (4 mL) was added dropwise at r.t. After 18 h, DCM (10 mL) and 1 N HCl (10 mL) were added and the mixture was stirred for 5 min. The organic phase was separated and the water phase was extracted with DCM (2 × 10 mL). The combined organic extract was dried over anhydrous  $\text{Na}_2\text{SO}_4$ , filtered and evaporated *in vacuo*. Purification by FLC afforded **13** (170 mg, 79%) as a dark orange oil that solidified upon standing at r.t.

For **13**:  $R_F = 0.26$  ( $\text{EtOAc}$ ), mp 223–225 °C; ESI-MS ( $m/z$ ) = 341.26 [ $\text{M} + 1$ ] $^+$ ; IR (ATR)  $\nu_{\text{max}}$  3377, 3356, 3309, 2972, 2933, 2870, 1685, 1625, 1547, 1460, 1363, 1299, 1228, 1104, 752, 593, 550, 469  $\text{cm}^{-1}$ ; Anal. Calcd for  $\text{C}_{17}\text{H}_{32}\text{N}_4\text{O}_3$  $^{+}$  (340.25) C 59.97, H 9.47, N 16.46. Found C 59.83, H 9.35, N 16.28.

### Cyclic voltammetry

**Chemicals.** The stock solutions of compounds **1–13** ( $c = 1 \times 10^{-3} \text{ mol L}^{-1}$ ) in  $\text{H}_2\text{O}$ –MeOH (9/1, v/v) were used for the preparation of working solutions ( $1 \times 10^{-4} \text{ mol L}^{-1}$ ) for electrochemical measurements by dilution with aq. phosphate buffer solution (PBS) at pH = 7 as supporting electrolyte. The latter was prepared in the usual way by mixing an appropriate amount of monosodium phosphate monohydrate ( $\text{NaH}_2\text{PO}_4 \cdot \text{H}_2\text{O}$ ) and disodium phosphate heptahydrate ( $\text{Na}_2\text{HPO}_4 \cdot 7\text{H}_2\text{O}$ ). All chemicals (analytical-reagent grade) were

used without further purification. The aqueous solutions were made with doubly-distilled deionised water with a resistivity above 18  $\text{M}\Omega \text{ cm}$ .

**Electrochemical measurements.** The cyclic voltammetry (CV) measurements were performed using an AUTOLAB PGSTAT-302N (Metrohm Autolab B.V., The Netherlands) potentiostat/galvanostat equipped with a USB electrochemical interface connected to a three-electrode single compartment glass cell and personal computer for data storage and processing. NOVA 1.9 software was employed for elaboration and evaluation of all CV voltammograms. The glass electrochemical cell consisted of an Ag/AgCl (3 mol  $\text{L}^{-1}$  KCl) and Pt wire as reference and counter electrode, respectively. A paraffin impregnated graphite electrode (PIGE) with a diameter of 5 mm was used as the working electrode. The PIGE was polished with aluminium oxide (grain size = 0.3  $\mu\text{m}$ ) and rinsed with deionised water to obtain a fresh electrode surface before each experiment. The pH value of PBS was monitored with pH meter Model 215 (Denver Instrument, USA) with a combined glass electrode, which was regularly calibrated with standard buffer solutions. All the half-wave potentials ( $E_{1/2}$ ) are given against Ag/AgCl (3 mol  $\text{L}^{-1}$  KCl) reference electrode at an ambient temperature of  $25 \pm 1$  °C. The 20 mL of the supporting electrolyte containing an appropriate amount of the studied compound was added to the glass electrochemical cell. Before each measurement, ultrapure  $\text{N}_2$  ( $\text{O}_2 < 2$  ppm) was used to degas the solutions (10 min) and to provide an inert atmosphere inside the electrochemical cell. CV voltammograms were recorded in a potential range from  $-1$  to  $+1$  V with the use of optimised instrumental parameters as follows: a scan rate of  $0.1 \text{ V s}^{-1}$ , a step potential of 0.005 V and an interval time of 0.05 s. At the beginning, the current response for a blank (PBS at pH = 7 without the presence of any studied nitroxide) was measured to check the electrochemical background of the system. Subsequently, CV voltammograms of each studied species were carried out fivefold ( $n = 5$ ) and the average scan was considered for the evaluation of  $E_{1/2}$  and construction of CV figures.

### Electron paramagnetic resonance

The stock solutions of all nitroxides were prepared in anhydrous dichloromethane (Merck, SeccoSolv®, max. 0.004%  $\text{H}_2\text{O}$ ), dimethylsulfoxide (Merck, SeccoSolv®, max. 0.025%  $\text{H}_2\text{O}$ ) and/or *n*-heptane (Merck, Uvasol®). EPR spectra were measured with freshly diluted solutions ( $c$  0.1 mM) carefully saturated with argon and immediately transferred to a small quartz flat cell (WG 808-Q, Wilmad-LabGlass, USA) optimised for the TE<sub>102</sub> cavity (Bruker, Germany). The X-band spectra were recorded using an EPR spectrometer EMX Plus (Bruker, Germany) at 295 K; in DMSO the EPR spectra were measured within the temperature range of 298 K–373 K. The temperature was set using a Bruker temperature control unit ER 4111 VT. The *g*-values were determined using a built-in magnetometer. Typical EPR spectrometer settings were as follows: microwave frequency: 9.428 GHz; microwave power: 1.053 mW or 10.53 mW; center field: 335.8 mT; sweep width: 6–10 mT; gain:

$5 \times 10^3$ ; modulation amplitude: 0.02 mT; scan: 82 s; time constant: 10.24 ms; number of scans: 5.

The experimental EPR spectra were analysed and simulated using the Bruker software WinEPR and SimFonia, Winsim2002 software.<sup>40</sup> The simulated spectra of dinitroxides were calculated with the EasySpin software package<sup>41</sup> using the fitting function pepper suitable for the exchange coupling constant calculation in systems with  $S > 1/2$ .

### X-ray analyses

Single-crystal X-ray diffraction experiments were made at the 293(1) K temperature on Oxford Gemini R (for **5** and **10**) or Xcalibur S (for **4**, **8**, and **11-0.5EtOH-0.5H<sub>2</sub>O**) four circle  $\kappa$ -axis diffractometers equipped with Ruby or Sapphire 2 CCD detectors and graphite monochromated Mo K $\alpha$  radiation. Crystal data, data collection procedures, structure determination methods and refinement results are summarised in Table S1 (see ESI†). CrysAlis program package<sup>42</sup> was used for data reduction. The structures were solved by direct methods using programs Shelxs97<sup>43</sup> and SIR2011,<sup>44</sup> or a charge-flipping method using program OLEX2.SOLVE.<sup>45</sup> Refinement was carried out on  $F^2$  and scattering factors were incorporated in ShelXL97, ShelXL2013 or OLEX2.REFINE programs.<sup>45,47</sup> All non-hydrogen atoms were refined with anisotropic thermal parameters. All hydrogen atoms were found from the Fourier map and they were refined isotropically. The Diamond program package was used for molecular structure drawing.<sup>46</sup>

The *tert*-butyl group in mononitroxide **4** displaying a positional disorder (Fig. S3 in ESI†) was modelled in three positions using the OLEX program package<sup>45</sup> with occupancy factors of 0.62, 0.22 and 0.16.

The trifluoromethyl group in mononitroxide **8** is disordered around special positions of mirror. The discrete positional disorder of *gem*-dimethyl groups of **8** was also observed (Fig. S6 in ESI†). The trifluoromethyl group of **11-0.5EtOH-0.5H<sub>2</sub>O** is also disordered in two positions (Fig. S11 in ESI†) with occupancy factors of 0.67 and 0.33. The F and C atoms of disordered groups were modelled using DFIX and SADI restraints. The disordered ethanol in the structure of **11-0.5EtOH-0.5H<sub>2</sub>O** residing in the special position (PART-1) was calculated using FRAG 17, FEND and AFIX 176 commands and ethanol molecule coordinates from Idealized Molecular Geometry Library.<sup>47</sup>

The atomic displacement parameters of C, O and F atoms were restrained using RIGU<sup>48</sup> and SIMU commands, and some atoms were also constrained using EADP command.

### Biological assays

The antibacterial activity of newly synthesised TEMPO radicals was evaluated by a broth micro-dilution method adapted from previous studies and in accordance with the NCCLS guidelines<sup>49</sup> on G<sup>+</sup> bacteria *Staphylococcus epidermidis* (Collection of Microorganisms at the Department of Biochemistry and Microbiology STU in Bratislava, Slovakia), *Staphylococcus aureus* CCM 3953 and G<sup>-</sup> bacteria *Proteus* sp. CCM 1977 (Czech Collection of Microorganisms, Masaryk University, Brno, Czech Republic).

Bacteria were grown in Mueller Hinton broth at 37 °C until an optical density (OD) of 0.8 at a wavelength of 630 nm was reached. The bacterial cultures were adjusted to equal the McFarland No. 0.5 turbidity standard. The final inoculum was prepared by diluting the adjusted bacterial suspension at 1:100 with Mueller Hinton broth, 198  $\mu$ L of inoculated broth was transferred to each well of the 96-well plate that contained 2  $\mu$ L of nitroxide radicals dissolved in DMSO (final concentrations 1–0.05 mmol L<sup>-1</sup>). The inoculated micro-plates were incubated at 37 °C until the growth reached the stationary phase. The antimicrobial activity was characterised by IC<sub>50</sub> and MIC values that were read from toxicity curves. The MIC was defined as the lowest concentration of the compound that inhibited the growth.

The antifungal assay was performed on yeast and filamentous fungi. Yeasts *Candida albicans* SC 5314 and *Candida parapsilosis* ATCC 22019 (American Type Culture Collection) were tested analogously to the antibacterial activity, however, the yeasts were grown in Sabouraud broth. The antifungal activity was evaluated based on IC<sub>50</sub> and MIC<sub>80</sub> values.<sup>50</sup>

Model filamentous fungi *Aspergillus fumigatus* CCM F-373, *Botrytis cinerea* CCM F-16 and *Fusarium culmorum* CCM F-21 were obtained from the Czech Collection of Microorganisms, Masaryk University, Brno, Czech Republic. These were tested by a macro-dilution technique on solidified growth medium potato-dextrose agar during static cultivation. Potato-dextrose growth media containing an appropriate concentration (1–0.1 mmol L<sup>-1</sup>) of tested nitroxide radicals were inoculated by fungal conidial suspension of tested fungi ( $1 \times 10^6$  conidia mL<sup>-1</sup>) in the centre of the growth media in Petri dishes. Fungi were cultivated<sup>51</sup> at 25 °C for 96 h. The radial growth was measured in millimeters. All experiments were performed in three parallels of two independent experiments.

## Acknowledgements

This work was supported by the Science and Technology Assistance Agency under contracts no. APVV-0014-11, APVV-0797-11, APVV-0282-10 and the Grant Agency of the Slovak Republic (VEGA 1/0051/13 and VEGA 1/0289/12).

## References

- (a) I. W. C. E. Arends, L. Yu-Xin, R. Ausan and R. Sheldon, *Tetrahedron*, 2006, **62**, 6659; (b) W. Yin, C. Chu, Q. Lu, J. Tao, X. Liang and R. Liu, *Adv. Synth. Catal.*, 2010, **352**, 113.
- 2,2,6,6-Tetramethylpiperidin-1-oxyl, in *Encyclopedia of Reagents for Organic Synthesis*, ed. F. Montanari, S. Quici, H. Henry-Riyad and T. T. Tidwell, Wiley-VCH, Weinheim, 2005.
- (a) M. F. Semmelhack, C. R. Schmid, D. A. Cortés and C. S. Chou, *J. Am. Chem. Soc.*, 1984, **106**, 3374; (b) P. Gamez, I. W. C. E. Arends, J. Reedijk and

- R. A. Sheldon, *Chem. Commun.*, 2003, 2414; (c) N. Merbouh, J. M. Bobbitt and Ch. Brückner, *Org. Prep. Proced. Int.*, 2004, **36**, 1; (d) J. M. Bobbitt, C. Brückner and N. Merbouh, *Org. React.*, 2009, **74**, 103; (e) S. Caron, R. W. Dugger, S. G. Ruggeri, J. A. Ragan and D. H. B. Ripin, *Chem. Rev.*, 2006, **106**, 2943; (f) R. Ciriminna and M. Pagliaro, *Org. Process Res. Dev.*, 2010, **14**, 245; (g) J. M. Hoover and S. S. Stahl, *J. Am. Chem. Soc.*, 2011, **133**, 16901; (h) S. Ma, J. Liu, S. Li, B. Chen, J. Cheng, J. Kuang, Y. Liu, B. Wan, Y. Wang, J. Ye, Q. Yu, W. Yuan and S. Yu, *Adv. Synth. Catal.*, 2011, **353**, 1005.
- 4 P.-Y. Blanchard, C. Niebel, S. Boisard, O. Alévêque, L. Sanguinet, M. Dias, T. Breton, Ch. Gautier and E. Levillan, *New J. Chem.*, 2012, **36**, 546.
- 5 M. Kavala, R. Boča, L. Dlhán, V. Brezová, M. Breza, J. Kožíšek, M. Fronc, P. Herich, L. Švorc and P. Szolcsányi, *J. Org. Chem.*, 2013, **78**, 6558.
- 6 *Nitroxides: Applications in Chemistry, Biomedicine, and Materials Science*, ed. G. Likhtenshtein, J. Yamauchi, S. Nakatsuji, A. I. Smirnov and R. Tamura, Wiley-VCH, Weinheim, 2008.
- 7 (a) K. Oyaizu and H. Nishide, *Adv. Mater.*, 2009, **21**, 2339; (b) J.-K. Kim, J.-H. Ahn, G. Cheruvally, G. S. Chauhan, J.-W. Choi, D.-S. Kim, H.-J. Ahn, S. H. Lee and Ch. E. Song, *Met. Mater. Int.*, 2009, **15**, 77; (c) K. Koshika, N. Chikushi, N. Sano, K. Oyaizu and H. Nishide, *Green Chem.*, 2010, **12**, 1573; (d) T. Janoschka, M. D. Hager and U. S. Schubert, *Adv. Mater.*, 2012, **24**, 6397.
- 8 (a) R. Chiarelli, M. A. Novak, A. Rassat and J. L. Tholence, *Nature*, 1993, **363**, 147; (b) Y. Wu, Y. Hirai, Y. Tsunobuchi, H. Tokoro, H. Eimura, M. Yoshio, S. Ohkoshi and T. Kato, *Chem. Sci.*, 2012, **3**, 3007.
- 9 (a) Z. Zhang, P. Chen, T. N. Murakami, S. M. Zakeeruddin and M. Grätzel, *Adv. Funct. Mater.*, 2008, **18**, 341; (b) F. Kato, N. Hayashi, T. Murakami, Ch. Okumura, K. Oyaizu and H. Nishide, *Chem. Lett.*, 2010, **39**, 464; (c) F. Kato, A. Kikuchi, T. Okuyama, K. Oyaizu and H. Nishide, *Angew. Chem., Int. Ed.*, 2012, **51**, 10177; (d) G. Grynova, J. M. Barakat, J. P. Blinco, S. E. Bottle and M. L. Coote, *Chem. – Eur. J.*, 2012, **18**, 7582.
- 10 P. Schattling, F. D. Jochum and P. Theato, *Chem. Commun.*, 2011, **47**, 8859.
- 11 (a) G. Sosnovsky, J. Lukszo, R. C. Brasch, U. G. Eriksson and T. N. Tozer, *Eur. J. Med. Chem.*, 1989, **24**, 241; (b) Z. Zhelev, R. Bakalova, I. Aoki, K. Matsumoto, V. Gadjeva, K. Anzai and I. Kanno, *Chem. Commun.*, 2009, 53.
- 12 (a) S. M. Hahn, Z. Tochner, C. M. Krishna, J. Glass, L. Wilson, A. Samuni, M. Sprague, D. Venzon, E. Glatstein, J. B. Mitchell and A. Russo, *Cancer Res.*, 1992, **52**, 1750; (b) A. P. Cotrim, F. Hyodo, K. Matsumoto, A. L. Sowers, J. A. Cook, B. J. Baum, M. C. Krishna and J. B. Mitchell, *Clin. Cancer Res.*, 2007, **13**, 4928; (c) M.-C. Frantz, J. G. Pierce, J. M. Pierce, L. Kangying, W. Qingwei, M. Johnson and P. Wipf, *Org. Lett.*, 2011, **13**, 2318.
- 13 J. M. Metz, D. Smith, R. Mick, R. Lustig, J. Mitchell, M. Cherakuri, E. Glatstein and S. M. Hahn, *Clin. Cancer Res.*, 2004, **10**, 6411.
- 14 (a) C. S. Wilcox and A. Pearlman, *Pharmacol. Rev.*, 2008, **60**, 418; (b) C. S. Wilcox, *Pharmacol. Ther.*, 2010, **126**, 119; (c) N. P. H. Tan, M. K. Taylor, S. E. Bottle, Ch. E. Wright, J. Ziogas, J. M. White, C. H. Schiesser and N. V. Jani, *Chem. Commun.*, 2011, **47**, 12083.
- 15 G. M. Rosen, E. Schneider, S. Shortkroff, P. Tsai and C. S. Winalski, *J. Chem. Soc., Perkin Trans. 1*, 2002, 2663.
- 16 Y. Ma, C. Lyons, P. Price and V. Chechik, *Org. Biomol. Chem.*, 2011, **9**, 5573.
- 17 D. Crich, D. Grant and A. A. Bowers, *J. Am. Chem. Soc.*, 2007, **129**, 12106.
- 18 D. Gravert, A. Datta, P. Wentworth Jr. and K. Janda, *J. Am. Chem. Soc.*, 1998, **120**, 9481.
- 19 J. Zakrzewski and J. Hupko, *Org. Prep. Proced. Int.*, 2003, **35**, 387.
- 20 J. Pirwitz and W. Damerau, *Z. Chem.*, 1976, **16**, 401.
- 21 Y. Basel and A. Hassner, *J. Org. Chem.*, 2000, **65**, 6368.
- 22 J. P. Blinco, J. L. Hodgson, B. J. Morrow, J. R. Walker, G. D. Will, M. L. Coote and S. E. Bottle, *J. Org. Chem.*, 2008, **73**, 6763.
- 23 (a) M. C. Krishna, D. A. Grahame, A. Samuni, J. B. Mitchell and A. Russo, *Proc. Natl. Acad. Sci. U. S. A.*, 1992, **89**, 5537; (b) E. J. Baur, S. Wang and M. C. Brandt, *Anal. Chem.*, 1996, **68**, 3815; (c) S. Goldstein, A. Samuni, K. Hideg and G. Merenyi, *J. Phys. Chem. A*, 2006, **110**, 3679.
- 24 G. Durand, F. Choteau, R. A. Prosak, A. Rockenbauer, F. A. Villamena and B. Puccia, *New J. Chem.*, 2010, **34**, 1909.
- 25 S. Morris, G. Sosnovsky, B. Hui, C. O. Huber, N. U. M. Rao and H. M. Swart, *J. Pharm. Sci.*, 1991, **80**, 149.
- 26 T. Yamasaki, Y. Matsuoka, F. Mito, M. Yamato and K. Yamada, *Asian J. Org. Chem.*, 2013, **2**, 388.
- 27 T. Isogai, T. Saito and A. Isogai, *Biomacromolecules*, 2010, **11**, 1593.
- 28 M. Jia, Y. Tang, Y.-F. Lam, S. A. Green and N. V. Blough, *Anal. Chem.*, 2009, **81**, 8033.
- 29 T. Yamasaki, F. Mito, Y. Ito, S. Pandian, Y. Kinoshita, K. Nakano, R. Murugesan, K. Sakai, H. Utsumi and K. Yamada, *J. Org. Chem.*, 2011, **76**, 435.
- 30 (a) P. H. Rieger, *Electron Spin Resonance Analysis and Interpretation*, RSC Publishing, Cambridge, UK, 2007; (b) M. F. Ottaviani, A. Modelli, O. Zeika, S. Jockusch, A. Moscatelli and N. J. Turro, *J. Phys. Chem. A*, 2012, **116**, 174; (c) S. H. Glarum and J. H. Marshall, *J. Chem. Phys.*, 1967, **47**, 1374; (d) V. N. Parmon, A. I. Kokorin and G. M. Zhidomirov, *J. Struct. Chem.*, 1977, **18**, 104; (e) G. Grampp, S. Landgraf, I. A. Grigorev, A. B. Shapiro and A. I. Kokorin, *Appl. Magn. Reson.*, 2000, **19**, 187; (f) G. Grampp, K. Rasmussen and A. I. Kokorin, *Appl. Magn. Reson.*, 2004, **26**, 245; (g) A. I. Kokorin, *Appl. Magn. Reson.*, 2004, **26**, 253; (h) A. I. Kokorin, V. A. Tran, K. Rasmussen and G. Grampp, *Appl. Magn. Reson.*, 2006, **30**, 35.
- 31 (a) V. N. Parmon and G. M. Zhidomirov, *Mol. Phys.*, 1974, **27**, 367; (b) V. N. Parmon, A. I. Kokorin, G. M. Zhidomirov

- and K. I. Zamaraev, *Mol. Phys.*, 1975, **30**, 695; (c) V. N. Parmon and G. M. Zhidomirov, *Mol. Phys.*, 1976, **32**, 613.
- 32 C. Ysacco, E. Rizzato, M.-A. Virolleaud, H. Karoui, A. Rockenbauer, F. Le Moigne, D. Siri, O. Ouari, R. G. Griffin and P. Tordo, *Phys. Chem. Chem. Phys.*, 2010, **12**, 5841.
- 33 (a) K. Komaguchi, T. Iida, Y. Goh, J. Ohshita, A. Kunai and M. Shiotani, *Chem. Phys. Lett.*, 2004, **387**, 327; (b) J. Szydłowska, K. Pietrasik, Ł. Głaz and A. Kaim, *Chem. Phys. Lett.*, 2008, **460**, 245; (c) C. Riplinger, J. P. Y. Kao, G. M. Rosen, V. Kathirvelu, G. R. Eaton, S. S. Eaton, A. Kutateladze and F. Neese, *J. Am. Chem. Soc.*, 2009, **131**, 10092.
- 34 F. R. Allen, *Acta Crystallogr., Sect. B: Struct. Sci.*, 2002, **58**, 380.
- 35 J. Bernstein, R. E. Devis, L. Shimoni and N.-L. Chang, *Angew. Chem., Int. Ed. Engl.*, 1995, **34**, 1555.
- 36 E. Torres, E. Moreno-Viguri, S. Galiano, G. Devarapally, P. W. Crawford, A. Azqueta, L. Arbillaga, J. Varela, E. Birriel, R. Di Maio, H. Cerecetto, M. González, I. Aldana, A. Monge and S. Pérez-Silanes, *Eur. J. Med. Chem.*, 2013, **66**, 324.
- 37 (a) C. Vilchéze, T. Hartman, B. Weinrick and W. R. Jacobs, *Nat. Commun.*, 2013, **4**, 1881; (b) G. Audran, P. Brémond, J.-M. Franconi, S. R. A. Marque, P. Massot, P. Mellet, P. Parzyb and E. Thiaudière, *Org. Biomol. Chem.*, 2014, **12**, 719.
- 38 J. Zakrzewski and M. Krawczyk, *Bioorg. Med. Chem. Lett.*, 2011, **21**, 514.
- 39 V. V. Tkachev, V. D. Sen and L. O. Atovmyan, *Bull. Acad. Sci. USSR, Div. Chem. Sci. (Engl. Transl.)*, 1987, **36**, 1696.
- 40 D. R. Duling, *J. Magn. Reson., Ser. B*, 1994, **104**, 105. (<http://www.niehs.nih.gov/research/resources/software/tox-pharm/tools/index.cfm>).
- 41 S. Stoll and A. Schweiger, *J. Magn. Reson.*, 2006, **178**, 42. (<http://www.easyspin.org>).
- 42 *CrysAlisPro, Version 1.171.36.20*, Oxford Diffraction Ltd, Abingdon, Oxford, England, 2012.
- 43 G. M. Sheldrick, *Acta Crystallogr., Sect. A: Found. Crystallogr.*, 2008, **64**, 112.
- 44 M. C. Burla, R. Caliendo, M. Camalli, B. Carrozini, G. L. Casciarano, C. Giacovazzo, M. Mallamo, A. Mazzone, G. Polidori and R. Spagna, *J. Appl. Crystallogr.*, 2012, **45**, 357.
- 45 O. V. Dolomanov, L. J. Bourhis, R. J. Gildea, J. A. K. Howard and H. Puschmann, *J. Appl. Crystallogr.*, 2009, **42**, 339.
- 46 K. Brandenburg and M. Berndt, *DIAMOND*, Crystal Impact GmbH, Bonn, Germany, 1999.
- 47 I. Guzei, *Idealized Molecular Geometry Library*, University of Wisconsin, Madison, USA, 2010.
- 48 A. Thorn, B. Dittrich and G. M. Sheldrick, *Acta Crystallogr., Sect. A: Found. Crystallogr.*, 2012, **68**, 448.
- 49 *Methods for Dilution Antimicrobial Susceptibility Tests for Bacteria That Grow Aerobically; Approved Standard—Fifth Edition*, Vol. 26, No. 2, USA, 2000.
- 50 *Reference Method for Broth Dilution Antifungal Susceptibility Testing of Yeasts; Approved Standard—Second Edition*, Vol. 22, No. 15, USA, 2002.
- 51 B. Dudová, D. Hudecová, R. Pokorný, M. Mičková, M. Palicová, P. Segla and M. Melník, *Folia Microbiol.*, 2002, **47**, 225.